

Efficient tensor decomposition method for noncircular source in colocated coprime MIMO radar

Qian-Peng Xie(谢前朋), Xiao-Yi Pan(潘小义), Shun-Ping Xiao(肖顺平)
Citation: Chin. Phys. B . 2020, 29(5): 054304 . **doi:** 10.1088/1674-1056/ab81f6
Journal homepage: http://cpb.iphy.ac.cn; http://iopscience.iop.org/cpb

What follows is a list of articles you may be interested in

High resolution inverse synthetic aperture radar imaging of three-axis-stabilized space target by exploiting orbital and sparse priors

Jun-Tao Ma(马俊涛), Mei-Guo Gao(高梅国), Bao-Feng Guo(郭宝锋), Jian Dong(董健), Di Xiong(熊娣), Qi Feng(冯祺)
Chin. Phys. B . 2017, 26(10): 108401 . **doi:** 10.1088/1674-1056/26/10/108401

Compensation of body shake errors in terahertz beam scanning single frequency holography for standoff personnel screening

Wei Liu(刘玮), Chao Li(李超), Zhao-Yang Sun(孙兆阳), Yu Zhao(赵宇), Shi-You Wu(吴世有), Guang-You Fang(方广有)
Chin. Phys. B . 2016, 25(8): 088402 . **doi:** 10.1088/1674-1056/25/8/088402

Research on spatial-variant property of bistatic ISAR imaging plane of space target

Guo Bao-Feng, Wang Jun-Ling, Gao Mei-Guo, Shang Chao-Xuan, Fu Xiong-Jun
Chin. Phys. B . 2015, 24(4): 048402 . **doi:** 10.1088/1674-1056/24/4/048402

Modified GIT model for predicting wind-speed behavior of low-grazing-angle radar sea clutter

Zhang Yu-Shi, Zhang Jin-Peng, Li Xin, Wu Zhen-Sen
Chin. Phys. B . 2014, 23(10): 108402 . **doi:** 10.1088/1674-1056/23/10/108402

Efficient tensor decomposition method for noncircular source in colocated coprime MIMO radar*

Qian-Peng Xie(谢前朋), Xiao-Yi Pan(潘小义)†, and Shun-Ping Xiao(肖顺平)

National University of Defense Technology, Changsha 410073, *China*

(Received 4 December 2019; revised manuscript received 2 February 2020; accepted manuscript online 23 March 2020)

An effective method via tensor decomposition is proposed to deal with the joint direction-of-departure (DOD) and direction-of-arrival (DOA) estimation of noncircular sources in colocated coprime MIMO radar. By decomposing the transmitter and receiver into two sparse subarrays, noncircular property of source can be used to construct new extended received signal model for two sparse subarrays. The new received model can double the virtual array aperture due to the elliptic covariance of imping sources is nonzero. To further exploit the multidimensional structure of the noncircular received model, we stack the subarray output and its conjugation according to mode-1 unfolding and mode-2 unfolding of a third-order tensor, respectively. Thus, the corresponding extended tensor model consisted of noncircular information for DOA and DOD can be obtained. Then, the higher-order singular value decomposition technique is utilized to estimate the accurate signal subspace and angular parameter can be automatically paired via the rotational invariance relationship. Specifically, the ambiguous angle can be eliminated and the true targets can be achieved with the aid of the coprime property. Furthermore, a closed-form expression for the deterministic CRB under the NC sources scenario is also derived. Simulation results verify the superiority of the proposed estimator.

Keywords: colocated coprime MIMO radar, noncircular signal, tensor decomposition, DOD and DOA estimation

PACS: 43.60.Jn, 43.60.Cg, 84.40.Xb **DOI:** 10.1088/1674-1056/ab81f6

1. Introduction

In recent years, the issue of angle parameter estimation in multiple-input multiple-output (MIMO) radar has become a hot research topic due to its broad applications in wireless communications, radar, sonar and navigation.[1–6] MIMO radar together with waveform diversity can exhibit higher resolution, better parameter identifiability, greater flexibility in the beampattern design, and more degrees of freedom (DOFs) over the conventional phased-array radar associated with coherent waveform. According to the deployment of transmit array and receive array, MIMO radar is generally categorised into statistical MIMO radar and colocated MIMO radar.[7,8] Furthermore, the colocated MIMO radar can be divided into bistatic and monostatic MIMO radar. For bistatic MIMO radar system, the direction-of-departure (DOD) and direction-of-arrival (DOA) are different, while the DOD and DOA are the same for monostatic MIMO radar because the transmitter and receiver are closely enough. In this work, our task is to investigate the DOD and DOA estimation for locating multiples targets in the bistatic MIMO radar system.

In order to determine DOD and DOA estimations in bistatic MIMO radar, many excellent methods have been proposed. In Refs. [9] and [10], peak searching methods are proposed to estimate the DOD and DOA, which demand high computational complexity. In order to avoid the downside of the peak searching methods, a polynomial root finding algorithm with automatical angular pairing is proposed in Ref. [11] for jointly estimating of DOD and DOA. In Ref. [12], the rotational invariance technique is proposed for angle parameter estimation in bistatic MIMO radar. Furthermore, a modified ESPRIT algorithm in Ref. [13] is presented to avoid the angle pairing process. In Ref. [14], by using the temporal uncorrelated characteristic of the spatial colored noise, a special fourth-order tensor structure is constructed to suppress the effect of colored noise in bistatic MIMO radar system. In Ref. [15], a beamspace-based technique by focusing transmitted energy within the desired spatial sector is proposed to improve the DOD and DOA estimation performance. The Sigmoid transform method is investigated to improve the joint DOD and DOA estimation performance for wideband bistatic MIMO radar system in the condition of impulsive noise environment in Ref. [16]. In order to deal with the antennas failure problem in bistatic MIMO radar, image entropy and low rank block hankel structured matrix completion method is proposed to recover the successive missing data.[17] In Ref. [18], by exploting the multidimensional structure inherented in the received data, the PARAFAC techqnique is adopted to achieve accuracy angle estimation in the presence of gain-phase error for bistatic MIMO radar.

However, all the methods mentioned above assume that both the transmit and receive arrays in bistatic MIMO radar are uniform linear array with half-wavelength spacing. To fur-

*Project supported by the National Natural Science Foundation of China (Grant Nos. 61701507, 61890542, and 61890540).

†Corresponding author. E-mail: mrpanxy@nudt.edu.cn

© 2020 Chinese Physical Society and IOP Publishing Ltd

ther improve the number of degrees of freedom (DOFs) and estimated resolution, it is necessary to design sparse transmit and receive arrays in MIMO radar. In Ref. [19], a new nested array configuration in transmit and receive side is proposed to enhance the number of DOFs of difference coarray of the sum coarray (DCSC). In Ref. [20], a coprime MIMO radar is designed to deal with the DOAs estimation of mixed coherent and uncorrelated sources, where the transmit array and receive array are the first sparse subarray and the second sparse subarray of a generalized coprime array, respectively. In Ref. [21], symmetric coprime array MIMO radar configuration is used to extend the maximum consecutive lags in the differece coarray domain of symmetric sum coarray after vectorizing the sample covariance matrix. But, the designed coprime or nested array configurations in Refs. [19–21] mainly improve the DOA estimation performance for monostatic MIMO radar. Different from the monostatic MIMO radar, the DOD and DOA in bistatic MIMO radar are different, causing more angle parameters to be estimated. In order to make full use of the advantages of coprime/nested array in bistatic MIMO radar, consective difference coarray corresponding to DOD and DOA are achieved by extracting specified covariance matrix elements in Ref. [22]. Although the sparse array configurations used in Refs. [19–22] can improve the angle estimation accuracy, the methods to estimate the DOD and DOA mainly focus on the difference coarray of the nested array or coprime array. According to Refs. [23–25], there exist two subararys both for nested array and coprime array. As analyzed in Refs. [26–28], high resolution angle parameter estimation can be obtained by exploiting the results of the two sparse subarrays in coprime array. Thus, we can improve the DOD and DOA estimation perforamce for bistatic coprime MIMO radar by dividing the coprime array in transmit and receive side into two uniform sparse linear subarrays. In Ref. [29], a partial spectral search (PSS) method is proposed to realize the two-dimensional (2D) DOA estimation for coprime plannar arrays (CPA), but, a tremendous computational burden is inevitable due to the 2D partial spectrum peak searching process. In order to alleviate the computation complexity, a computationally efficient one-dimensional (1D) PSS method via reduced dimensional transform in Ref. [30] is conducted to 2D DOA estimation for CPA. In Ref. [31], a parallel factor (PARAFAC) model is constrcuted by using the multidimensional structure inherent in the received data of each subarray and the convergence speed of the proposed PARAFAC algorithm is fast via propagator method (PM) as the initialization of the angle estimation. The proposed methods in Refs. [29–31] can also be applied to joint DOD and DOA estimations in bistatic coprime MIMO radar becasue the received signal model in CPA is similar with the model in bistatic coprime MIMO radar. However, all the mentioned algorithms in Refs. [29–31] ignore the noncircular characteristic of the imping sources when estimate the angle parameter for CPA. It is well known that the angle estimaiton accuracy and resolved sources can be significant improved by using noncircular characteristic of the noncircular signals.[32] In this paper, we improve the DOD and DOA estimation performance for bistatic coprime MIMO radar with the aid of the noncircular characteristic. By combining the noncircular characteristic and bistatic coprime MIMO radar, two new extend three-order tensor models corresponding to DOD and DOA can be constructed by exploiting the multidimensional inherent structure. And, high accuracy novel signal subspace matrices can be obtained by using the multi-SVD method. Then, the rotational invaraince technique can be used and the estimated DODs and DOAs are automatically paired. Furthermore, all the DODs and DOAs can be achieved by utilising the linear relationship between the true and ambiguous angle parameter and the true estimated DODs and DOAs can be obtained by using the coprime property. The effectiveness and superiority of the proposed algorithm are verified by numerical simulation in Section 5.

The main contributions of this work can be summarized below.

(i) Two new three order tensor signal models corresponding to DOD and DOA are constructed, which can make full use of the noncircular characteristic inherent in the impinging sources.

(ii) Accurate signal subspace matrices are obtained by performing multi-SVD on new three-order tensor signal models and automatically paired estimated DODs and DOAs are identified by using the rotational invaraince technique. Furthermore, accuracy estimated true DODs and DOAs can be obtained by eliminating the ambiguous angles with the help of the coprime property.

(iii) The proposed method can avoid spectrum peak searching processing compared with the PSS method and extend the array aperture compared with the PARAFAC method by using the noncircualr characteristic.

The rest of this paper is organized as follows. In Section 2, system model is addressed. In Section 3, we describe the proposed tensor-based method for DOD and DOA estimations. In Section 4, the performance analysis about computational complexity, identified targets, and CRB is discussed. In Section 5, the performance of the proposed method is evaluated through extensive simulations and Section 6 concludes the paper.

Notations: Throughout this paper, scalars, vectors, and matrices are denoted by lowercase letters, boldface lowercase letters, and boldface uppercase letters, respectively. The superscripts $*$, T, and H denote the complex conjugate, the transpose, and the complex conjugate transpose, respectively. The Moore–Penrose pseudoinverse is denoted by the superscript

dagger †. The symbols $\otimes$, $\odot$, and $\oplus$ denote the Kronecker product, Kronecker–Rao operation, and Hadamard product, respectively. The diag$(\cdot)$ or $\boldsymbol{D}_n$ denotes a diagonal matrix. Additionally, $\boldsymbol{0}$ and $\boldsymbol{I}$ denote the zero matrix and identity matrix with appropriate dimension.

2. System model

Consider a bistatic MIMO radar system with M transmit array and N receive array to locate K targets in the 2D detection area. As illustrated in Fig. 1, the transmitter and receiver are omnidirectional coprime linear arrays and both of them can be separated into two undersampled uniform linear subarrays. In this paper, we consider $M=N$, $M_1=N_1$, and $M_2=N_2$. Both for the transmit array and receive array, the first subarray contains M_2 sensors with adjacent interval being $M_1 d$, while the second subarray contains M_1 sensors with adjacent interval being $M_2 d$, where the unit inter-element spacing d is set to $\lambda/2$, and λ denotes the wavelength. The element positions of the corresponding transmit and receive array can be denoted as

$$\mathbb{P}=\{M_1 md|0\le m\le M_2\}\cup\{M_2 md|0\le m\le M_1\}. \quad (1)$$

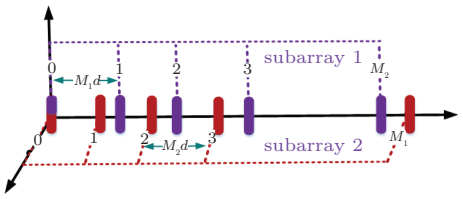


Fig. 1. Illustration of the transmit (receive) array of a bistatic coprime MIMO radar system.

The transmitter utilizes the M arrays to emit different narrowband orthogonal noncircular signals, which have the identifical bandwidth and center frequency. Assume there are K narrowband far-field uncorrelated sources with (θ_k,ϕ_k), $k=1,2,\ldots,K$, where θ_k and ϕ_k denotes the DOD and DOA of the k-th sources, respectively. Thus, the signal model in the receiving end can be expressed as

$$\boldsymbol{X}(t)=\sum_{k=1}^{K}\beta_k\boldsymbol{b}(\phi_k)\boldsymbol{a}^{\mathrm{T}}(\theta_k)\boldsymbol{U}+\boldsymbol{W}(t), \quad (2)$$

where $\boldsymbol{b}(\phi_k)=[1,\mathrm{e}^{-\mathrm{j}\pi d_{r1}\sin(\phi_k)},\ldots,\mathrm{e}^{\mathrm{j}\pi d_{rN}\sin(\phi_k)}]^{\mathrm{T}}\in\mathbb{C}^{N\times 1}$ is the steering vector corresponding to DOA and $\boldsymbol{a}(\theta_k)=[1,\mathrm{e}^{-\mathrm{j}\pi d_{t1}\sin(\theta_k)},\ldots,\mathrm{e}^{\mathrm{j}\pi d_{tM}\sin(\theta_k)}]^{\mathrm{T}}\in\mathbb{C}^{M\times 1}$ is the steering vector corresponding to DOD. β_k denotes the reflection coefficients of K targets; $\boldsymbol{U}$ is the emitted orthogonal noncircular waveforms; $\boldsymbol{W}$ denotes the additive Gaussian white noise. By exploiting the orthogonality between the transmit and receive waveforms, the received data after the matched filtering operation can be written as

$$\begin{aligned}\bar{\boldsymbol{X}}(t)&=\sum_{k=1}^{K}\beta_k\boldsymbol{b}(\phi_k)\boldsymbol{a}^{\mathrm{T}}(\theta_k)\boldsymbol{U}\boldsymbol{U}^{\mathrm{H}}+\boldsymbol{W}(t)\boldsymbol{U}^{\mathrm{H}}\\&=\sum_{k=1}^{K}\beta_k\mathrm{e}^{\mathrm{j}\psi_k}s_{0k}(t)\boldsymbol{b}(\phi_k)\boldsymbol{a}^{\mathrm{T}}(\theta_k)+\bar{\boldsymbol{W}}(t)\\&=\boldsymbol{B}(\phi)\boldsymbol{\Lambda}\boldsymbol{A}^{\mathrm{T}}(\theta)+\bar{\boldsymbol{W}}(t),\end{aligned} \quad (3)$$

where

$$\boldsymbol{\Lambda}=\mathrm{diag}[\beta_1\mathrm{e}^{\mathrm{j}\psi_1}s_{01}(t),\beta_2\mathrm{e}^{\mathrm{j}\psi_2}s_{02}(t),\ldots,\beta_K\mathrm{e}^{\mathrm{j}\psi_K}s_{0K}(t)]$$

denotes the noncircular baseband signal corresponding to the k-th target, ψ_k and $s_{0k}(t)$ denote noncircular phase and the real part of the noncircular signal.

$$\begin{aligned}\boldsymbol{B}(\phi)&=[\boldsymbol{b}(\phi_1),\boldsymbol{b}(\phi_2),\ldots,\boldsymbol{b}(\phi_K)],\\\boldsymbol{A}(\theta)&=[\boldsymbol{a}(\theta_1),\boldsymbol{a}(\theta_2),\ldots,\boldsymbol{a}(\theta_K)]\end{aligned}$$

denote the receive and transmit steering matrices, respectively. By vectorizing $\bar{\boldsymbol{X}}(t)$ in Eq. (3), the output of the matched filtering can be rewritten as

$$\boldsymbol{y}(t)=(\boldsymbol{A}(\theta)\odot\boldsymbol{B}(\phi))\boldsymbol{s}(t)+\boldsymbol{n}(t), \quad (4)$$

where

$$\begin{aligned}\boldsymbol{s}(t)&=\mathrm{diag}(\boldsymbol{\Lambda})\\&=[\beta_1\mathrm{e}^{\mathrm{j}\psi_1}s_{01}(t),\beta_2\mathrm{e}^{\mathrm{j}\psi_2}s_{02}(t),\ldots,\beta_K\mathrm{e}^{\mathrm{j}\psi_K}s_{0K}(t)]^{\mathrm{T}},\end{aligned}$$

$\boldsymbol{n}(t)=\mathrm{vec}(\bar{\boldsymbol{W}}(t))$ denotes the additive Gaussian white noise vector with covariance matrix $\sigma^2\boldsymbol{I}_{MN\times 1}$. By collecting all snapshots together, the received data becomes

$$\begin{aligned}\boldsymbol{Y}&=(\boldsymbol{A}(\theta)\odot\boldsymbol{B}(\phi))\boldsymbol{S}+\boldsymbol{N}\\&=\begin{bmatrix}\boldsymbol{A}(\theta)\boldsymbol{D}_1(\boldsymbol{B}(\phi))\\\boldsymbol{A}(\theta)\boldsymbol{D}_2(\boldsymbol{B}(\phi))\\\vdots\\\boldsymbol{A}(\theta)\boldsymbol{D}_N(\boldsymbol{B}(\phi))\end{bmatrix}\boldsymbol{S}+\boldsymbol{N},\end{aligned} \quad (5)$$

where $\boldsymbol{D}_n$ denotes a diagonal matrix that uses the n-th row of the matrix; $\boldsymbol{S}=\boldsymbol{\Xi}\boldsymbol{S}_0$ denotes the multiple snapshots noncircular baseband signal, $\boldsymbol{\Xi}=\mathrm{diag}(\mathrm{e}^{\mathrm{j}\psi_1},\mathrm{e}^{\mathrm{j}\psi_2},\ldots,\mathrm{e}^{\mathrm{j}\psi_K})$, and $\boldsymbol{S}_0$ denotes the real part of $\boldsymbol{S}$. In order to exploit the noncircularity characteristic, we extend the array output by stacking the received data and its conjugation as follows:

$$\begin{aligned}\boldsymbol{Y}_{\mathrm{nc}}&=\begin{bmatrix}\boldsymbol{Y}\\\boldsymbol{J}\boldsymbol{Y}^*\end{bmatrix}\\&=\begin{bmatrix}(\boldsymbol{A}(\theta)\odot\boldsymbol{B}(\phi))\boldsymbol{S}\\\boldsymbol{J}(\boldsymbol{A}(\theta)\odot\boldsymbol{B}(\phi)\boldsymbol{S})^*\end{bmatrix}+\begin{bmatrix}\boldsymbol{N}\\\boldsymbol{J}\boldsymbol{N}^*\end{bmatrix}\\&=\begin{bmatrix}(\boldsymbol{A}(\theta)\odot\boldsymbol{B}(\phi))\boldsymbol{\Xi}\boldsymbol{S}_0\\\boldsymbol{J}(\boldsymbol{A}(\theta)\odot\boldsymbol{B}(\phi)\boldsymbol{\Xi}\boldsymbol{S}_0)^*\end{bmatrix}+\tilde{\boldsymbol{N}}\\&=\begin{bmatrix}(\boldsymbol{A}(\theta)\odot\boldsymbol{B}(\phi))\boldsymbol{\Xi}\\\boldsymbol{J}(\boldsymbol{A}(\theta)\odot\boldsymbol{B}(\phi)\boldsymbol{\Xi})^*\end{bmatrix}\boldsymbol{S}_0+\tilde{\boldsymbol{N}}\\&=\boldsymbol{A}_{nc}\boldsymbol{S}_0+\tilde{\boldsymbol{N}},\end{aligned} \quad (6)$$

where $\boldsymbol{J}\in\mathbb{R}^{MN\times MN}$ denotes the permutation matrix with ones on its anti-diagonal and zeros elsewhere; $\boldsymbol{A}_{\mathrm{nc}}\in\mathbb{C}^{2MN\times K}$ denotes the extended joint steering matrix, which has the following form:

$$
\begin{aligned}
\boldsymbol{A}_{nc} &= \begin{bmatrix} (\boldsymbol{A}(\theta)\odot\boldsymbol{B}(\phi))\boldsymbol{\Xi} \\ \boldsymbol{J}(\boldsymbol{A}(\theta)\odot\boldsymbol{B}(\phi)\boldsymbol{\Xi})^* \end{bmatrix} = \begin{bmatrix} \boldsymbol{A}(\theta)\boldsymbol{\Xi}\boldsymbol{D}_1(\boldsymbol{B}(\phi)) \\ \boldsymbol{A}(\theta)\boldsymbol{\Xi}\boldsymbol{D}_2(\boldsymbol{B}(\phi)) \\ \vdots \\ \boldsymbol{A}(\theta)\boldsymbol{\Xi}\boldsymbol{D}_N(\boldsymbol{B}(\phi)) \\ \boldsymbol{J}_1(\boldsymbol{A}^*(\theta)\boldsymbol{D}_1(\boldsymbol{B}(\phi)^*)\boldsymbol{\Xi}^*) \\ \boldsymbol{J}_1(\boldsymbol{A}^*(\theta)\boldsymbol{D}_2(\boldsymbol{B}(\phi)^*)\boldsymbol{\Xi}^*) \\ \vdots \\ \boldsymbol{J}_1(\boldsymbol{A}^*(\theta)\boldsymbol{D}_N(\boldsymbol{B}(\phi)^*)\boldsymbol{\Xi}^*) \end{bmatrix} \\
&= \begin{bmatrix} \boldsymbol{A}(\theta)\boldsymbol{\Xi}\boldsymbol{D}_1(\boldsymbol{B}(\phi)) \\ \boldsymbol{A}(\theta)\boldsymbol{\Xi}\boldsymbol{D}_2(\boldsymbol{B}(\phi)) \\ \vdots \\ \boldsymbol{A}(\theta)\boldsymbol{\Xi}\boldsymbol{D}_N(\boldsymbol{B}(\phi)) \\ (\boldsymbol{A}(\theta)\boldsymbol{\Psi}\boldsymbol{D}_1(\boldsymbol{B}(\phi))\boldsymbol{\Phi}\boldsymbol{\Xi}_1) \\ (\boldsymbol{A}(\theta)\boldsymbol{\Psi}\boldsymbol{D}_2(\boldsymbol{B}(\phi))\boldsymbol{\Phi}\boldsymbol{\Xi}_1) \\ \vdots \\ (\boldsymbol{A}(\theta)\boldsymbol{\Psi}\boldsymbol{D}_N(\boldsymbol{B}(\phi))\boldsymbol{\Phi}\boldsymbol{\Xi}_1) \end{bmatrix} = \begin{bmatrix} \boldsymbol{A}(\theta)\boldsymbol{\Xi}\boldsymbol{D}_1(\boldsymbol{B}(\phi)) \\ \boldsymbol{A}(\theta)\boldsymbol{\Xi}\boldsymbol{D}_2(\boldsymbol{B}(\phi)) \\ \vdots \\ \boldsymbol{A}(\theta)\boldsymbol{\Xi}\boldsymbol{D}_N(\boldsymbol{B}(\phi)) \\ (\boldsymbol{A}(\theta)\boldsymbol{\Psi}\boldsymbol{\Phi}\boldsymbol{\Xi}_1)\boldsymbol{D}_1(\boldsymbol{B}(\phi)) \\ (\boldsymbol{A}(\theta)\boldsymbol{\Psi}\boldsymbol{\Phi}\boldsymbol{\Xi}_1)\boldsymbol{D}_2(\boldsymbol{B}(\phi)) \\ \vdots \\ (\boldsymbol{A}(\theta)\boldsymbol{\Psi}\boldsymbol{\Phi}\boldsymbol{\Xi}_1)\boldsymbol{D}_N(\boldsymbol{B}(\phi)) \end{bmatrix} \\
&= \begin{bmatrix} (\boldsymbol{A}(\theta)\boldsymbol{\Xi})\odot\boldsymbol{B}(\phi) \\ (\boldsymbol{A}(\theta)\boldsymbol{\Psi}\boldsymbol{\Phi}\boldsymbol{\Xi}_1)\odot\boldsymbol{B}(\phi) \end{bmatrix},
\end{aligned} \tag{7}
$$

where

$$
\boldsymbol{\Psi} = \mathrm{diag}[\mathrm{e}^{\mathrm{j}\pi d_{rM}\sin(\theta_1)}, \mathrm{e}^{\mathrm{j}\pi d_{rM}\sin(\theta_2)}, \ldots, \mathrm{e}^{\mathrm{j}\pi d_{rM}\sin(\theta_K)}],
$$

$$
\boldsymbol{\Phi} = \mathrm{diag}[\mathrm{e}^{\mathrm{j}\pi d_{tN}\sin(\phi_1)}, \mathrm{e}^{\mathrm{j}\pi d_{tN}\sin(\phi_2)}, \ldots, \mathrm{e}^{\mathrm{j}\pi d_{tN}\sin(\phi_K)}], \qquad \boldsymbol{\Xi}_1 = \mathrm{diag}[\mathrm{e}^{\mathrm{j}\psi_K}, \mathrm{e}^{\mathrm{j}\psi_{K-1}}, \ldots, \mathrm{e}^{\mathrm{j}\psi_1}].
$$

From Eq. (7), we can find that the non-circularity characteristics can extend the steering matrix corresponding to DOD. Here, we also demonstrate that the non-circularity characteristics can extend the steering matrix corresponding to DOA.

For matrices $\boldsymbol{A}\in\mathbb{C}^{M\times K}$, $\boldsymbol{B}\in\mathbb{C}^{N\times K}$, and $\boldsymbol{K}\in\mathbb{R}^{MN\times MN}$, using the commutative relationship of Kronecker–Rao operation, we can obtained that $\boldsymbol{A}\odot\boldsymbol{B} = \boldsymbol{K}(\boldsymbol{B}\odot\boldsymbol{A})$. Therefore, we can find that there exists a transform relationship between the extend joint steering matrix for DOA and DOD as follows:

$$
\begin{aligned}
\boldsymbol{B}_{\mathrm{nc}} &= \begin{bmatrix} \boldsymbol{K} & \\ & \boldsymbol{J}\boldsymbol{K}\boldsymbol{J} \end{bmatrix} \boldsymbol{A}_{\mathrm{nc}} = \begin{bmatrix} \boldsymbol{K}(\boldsymbol{A}(\theta)\odot\boldsymbol{B}(\phi))\boldsymbol{\Xi} \\ \boldsymbol{J}\boldsymbol{K}\boldsymbol{J}(\boldsymbol{A}(\theta)\odot\boldsymbol{B}(\phi)\boldsymbol{\Xi})^* \end{bmatrix} = \begin{bmatrix} \boldsymbol{K}(\boldsymbol{A}(\theta)\odot\boldsymbol{B}(\phi))\boldsymbol{\Xi} \\ \boldsymbol{J}(\boldsymbol{K}\boldsymbol{A}(\theta)\odot\boldsymbol{B}(\phi)\boldsymbol{\Xi})^* \end{bmatrix} \\
&= \begin{bmatrix} \boldsymbol{K}(\boldsymbol{A}(\theta)\odot\boldsymbol{B}(\phi))\boldsymbol{\Xi} \\ \boldsymbol{J}(\boldsymbol{K}\boldsymbol{A}(\theta)\odot\boldsymbol{B}(\phi)\boldsymbol{\Xi})^* \end{bmatrix} = \begin{bmatrix} (\boldsymbol{B}(\phi)\odot\boldsymbol{A}(\theta))\boldsymbol{\Xi} \\ \boldsymbol{J}(\boldsymbol{B}(\phi)\odot\boldsymbol{A}(\theta)\boldsymbol{\Xi})^* \end{bmatrix} = \begin{bmatrix} \boldsymbol{B}(\phi)\boldsymbol{\Xi}\boldsymbol{D}_1(\boldsymbol{A}(\theta)) \\ \boldsymbol{B}(\phi)\boldsymbol{\Xi}\boldsymbol{D}_2(\boldsymbol{A}(\theta)) \\ \vdots \\ \boldsymbol{B}(\phi)\boldsymbol{\Xi}\boldsymbol{D}_M(\boldsymbol{A}(\theta)) \\ \boldsymbol{J}_1(\boldsymbol{B}(\phi)^*\boldsymbol{D}_1(\boldsymbol{A}(\theta))^*\boldsymbol{\Xi}^*) \\ \boldsymbol{J}_1(\boldsymbol{B}(\phi)^*\boldsymbol{D}_2(\boldsymbol{A}(\theta))^*\boldsymbol{\Xi}^*) \\ \vdots \\ \boldsymbol{J}_1((\boldsymbol{B}(\phi)^*\boldsymbol{D}_M(\boldsymbol{A}(\theta))^*\boldsymbol{\Xi}^*)) \end{bmatrix} \\
&= \begin{bmatrix} \boldsymbol{B}(\phi)\boldsymbol{\Xi}\boldsymbol{D}_1(\boldsymbol{A}(\theta)) \\ \boldsymbol{B}(\phi)\boldsymbol{\Xi}\boldsymbol{D}_2(\boldsymbol{A}(\theta)) \\ \vdots \\ \boldsymbol{B}(\phi)\boldsymbol{\Xi}\boldsymbol{D}_M(\boldsymbol{A}(\theta)) \\ (\boldsymbol{B}(\phi)\boldsymbol{\Phi}\boldsymbol{D}_1(\boldsymbol{A}(\theta)\boldsymbol{\Psi})\boldsymbol{\Xi}_1) \\ (\boldsymbol{B}(\phi)\boldsymbol{\Phi}\boldsymbol{D}_2(\boldsymbol{A}(\theta)\boldsymbol{\Psi})\boldsymbol{\Xi}_1) \\ \vdots \\ (\boldsymbol{B}(\phi)\boldsymbol{\Phi}\boldsymbol{D}_M(\boldsymbol{A}(\theta)\boldsymbol{\Psi}))\boldsymbol{\Xi}_1) \end{bmatrix} = \begin{bmatrix} \boldsymbol{B}(\phi)\boldsymbol{\Xi}\boldsymbol{D}_1(\boldsymbol{A}(\theta)) \\ \boldsymbol{B}(\phi)\boldsymbol{\Xi}\boldsymbol{D}_2(\boldsymbol{A}(\theta)) \\ \vdots \\ \boldsymbol{B}(\phi)\boldsymbol{\Xi}\boldsymbol{D}_M(\boldsymbol{A}(\theta)) \\ (\boldsymbol{B}(\phi)\boldsymbol{\Phi}\boldsymbol{\Psi}\boldsymbol{\Xi}_1)\boldsymbol{D}_1(\boldsymbol{A}(\theta)) \\ (\boldsymbol{B}(\phi)\boldsymbol{\Phi}\boldsymbol{\Psi}\boldsymbol{\Xi}_1)\boldsymbol{D}_2(\boldsymbol{A}(\theta)) \\ \vdots \\ (\boldsymbol{B}(\phi)\boldsymbol{\Phi}\boldsymbol{\Psi}\boldsymbol{\Xi}_1)\boldsymbol{D}_M(\boldsymbol{A}(\theta)) \end{bmatrix} \\
&= \begin{bmatrix} (\boldsymbol{B}(\phi)\boldsymbol{\Xi})\odot\boldsymbol{A}(\theta) \\ (\boldsymbol{B}(\phi)\boldsymbol{\Phi}\boldsymbol{\Psi}\boldsymbol{\Xi}_1)\odot\boldsymbol{A}(\theta) \end{bmatrix},
\end{aligned} \tag{8}
$$

where $\boldsymbol{T} = \mathrm{diag}[\boldsymbol{K}, \boldsymbol{JKJ}]$ denotes a nonsingular commutative matrix. Thus, the extend received signal model corresponding to DOD and DOA by using the first sparse subarray of the coprime MIMO radar can be represented as the following expressions

$$\boldsymbol{Y}_{1\mathrm{nc}} = \boldsymbol{A}_{\mathrm{nc}1}\boldsymbol{S}_0 + \tilde{\boldsymbol{N}}_1, \tag{9}$$

$$\boldsymbol{Y}_{2\mathrm{nc}} = \boldsymbol{B}_{\mathrm{nc}1}\boldsymbol{S}_0 + \tilde{\boldsymbol{N}}_2, \tag{10}$$

where

$$\boldsymbol{A}_{\mathrm{nc}1} = \begin{bmatrix} (\boldsymbol{A}_1(\theta)\boldsymbol{\Xi}) \odot \boldsymbol{B}_1(\phi), \\ (\boldsymbol{A}_1(\theta)\boldsymbol{\Psi}_1\boldsymbol{\Phi}_1\boldsymbol{\Xi}_1) \odot \boldsymbol{B}_1(\phi) \end{bmatrix}, \tag{11}$$

$$\boldsymbol{B}_{\mathrm{nc}1} = \begin{bmatrix} (\boldsymbol{B}_1(\phi)\boldsymbol{\Xi}) \odot \boldsymbol{A}_1(\theta) \\ (\boldsymbol{B}_1(\phi)\boldsymbol{\Phi}_1\boldsymbol{\Psi}_1\boldsymbol{\Xi}_1) \odot \boldsymbol{A}_1(\theta) \end{bmatrix}, \tag{12}$$

and

$$\boldsymbol{\Psi}_1 = \mathrm{diag}\left[\mathrm{e}^{\mathrm{j}\pi M_1(M_2-1)\sin(\theta_1)}, \mathrm{e}^{\mathrm{j}\pi M_1(M_2-1)\sin(\theta_2)}, \ldots, \mathrm{e}^{\mathrm{j}\pi M_1(M_2-1)\sin(\theta_K)}\right],$$

$$\boldsymbol{\Phi}_1 = \mathrm{diag}\left[\mathrm{e}^{\mathrm{j}\pi M_1(M_2-1)\sin(\phi_1)}, \mathrm{e}^{\mathrm{j}\pi M_1(M_2-1)\sin(\phi_2)}, \ldots, \mathrm{e}^{\mathrm{j}\pi M_1(M_2-1)\sin(\phi_K)}\right],$$

$$\boldsymbol{A}_1 = [\boldsymbol{a}_1(\theta_1), \boldsymbol{a}_1(\theta_2), \ldots, \boldsymbol{a}_1(\theta_K)] \in \mathbb{C}^{M_2\times K},$$

and $\boldsymbol{B}_1 = [\boldsymbol{b}_1(\phi_1), \boldsymbol{b}_1(\phi_2), \ldots, \boldsymbol{b}_1(\phi_K)] \in \mathbb{C}^{M_2\times K}$ is the steering matrix according to the i-th subarray of coprime array both in transmit and receive side. The direction steering vectors $\boldsymbol{a}_1(\theta_k)$ and $\boldsymbol{b}_1(\theta_k)$ satisfy

$$\boldsymbol{a}_1(\theta_k) = \left[1, \mathrm{e}^{\mathrm{j}\pi M_1\sin(\theta_k)}, \ldots, \mathrm{e}^{\mathrm{j}\pi M_1(M_2-1)\sin(\theta_k)}\right]^{\mathrm{T}}, \tag{13}$$

$$\boldsymbol{b}_1(\theta_k) = \left[1, \mathrm{e}^{\mathrm{j}\pi M_1\sin(\phi_k)}, \ldots, \mathrm{e}^{\mathrm{j}\pi M_1(M_2-1)\sin(\phi_k)}\right]^{\mathrm{T}}. \tag{14}$$

According to Eqs. (13) and (14), the ambiguous elimination problem needs to be considered due to that the adjacent interval of the first subarrays is larger than half wavelength. And, it is obvious that the extend received data model of the second subarray for DOD and DOA has the similar form as Eqs. (9) and (10). Therefore, in the following section, we only derive the solution for first subarray in detail. The solution for the second subarray can be delt with in the same way and the corresponding process is omitted in this paper.

3. The proposed method

3.1. Tensor definitions

Firstly, some tensor basics are introduced to better understand the multidimensional structure and the detailed introduction about the concept and operations of tensor can be found in Refs. [33,34].

Definition 1 (**Matrix unfolding**) For the N-th order tensor $\mathcal{X} \in \mathbb{C}^{I_1\times I_2\times\cdots\times I_N}$, its mode-$n$ unfolding can be indicated by $[\mathcal{X}]_{(n)} \in \mathbb{C}^{I_n\times(I_{n+1}\times\cdots I_N I_1\times(I_2\times\cdots I_{n-1})}$, where the $(i_1, i_2, \ldots, i_N)$-th element of $\mathcal{X}$ maps to the (i_n, j)-th element of $[\mathcal{X}]_{(n)}$, where

$$j = 1 + \sum_{k=1,k\neq n}^{N} (i_k - 1)J_k$$

with $J_k = \prod_{m=1,m\neq n}^{k-1} I_m$.

Definition 2 (**Mode-n tensor-matrix product**) The mode-n product of an N-order tensor $\mathcal{X} \in \mathbb{C}^{I_1\times I_2\times\cdots\times I_N}$ and a matrix $\boldsymbol{A} \in \mathbb{C}^{J\times I_n}$ is denoted by

$$\mathcal{Y} = \mathcal{X} \times_n \boldsymbol{A} \in \mathbb{C}^{I_1\cdots\times I_{n-1}\times J\times I_{n+1}\cdots\times I_N}$$

with

$$\mathcal{Y}_{i_1\cdots i_{n-1} j i_{n+1}\cdots i_N} = \sum_{i_n=1}^{I_n} \mathcal{X}_{i_1\cdots\times i_{n-1}\times i_{n+1}\cdots\times i_N} a_{j i_n}.$$

The mode product satisfies the following properties:

$$\mathcal{X} \times_m \boldsymbol{A} \times_n \boldsymbol{B} = \mathcal{X} \times_n \boldsymbol{B} \times_m \boldsymbol{A} \quad (m \neq n), \tag{15}$$

$$\mathcal{X} \times_m \boldsymbol{A} \times_m \boldsymbol{B} = \mathcal{X} \times_m (\boldsymbol{BA}), \tag{16}$$

$$[\mathcal{X} \times_1 \boldsymbol{A}_1 \times_2 \boldsymbol{A}_2 \times_{\ldots} \times_N \boldsymbol{A}_N]_{(n)} = \boldsymbol{A}_{(n)}\mathcal{X}_{(n)}[\boldsymbol{A}_{n+1} \otimes \cdots \otimes \boldsymbol{A}_N \otimes \boldsymbol{A}_1 \otimes \cdots \otimes \boldsymbol{A}_{n-1}]^{\mathrm{T}}. \tag{17}$$

Definition 3 (**Multi-SVD**) Multilinear SVD of an N-order tensor $\mathcal{X} \in \mathbb{C}^{I_1\times I_2\times\cdots\times I_N}$ can be denoted as $\mathcal{X} = \mathcal{G} \times_1 \boldsymbol{U}_1 \times_2 \boldsymbol{U}_2 \times_3 \cdots \times_N \boldsymbol{U}_N$, where $\boldsymbol{U}_n$ is the unitary matrix of the n-mode singular vectors satisfies $\mathcal{X}_n = \boldsymbol{U}_n\boldsymbol{\Sigma}_n\boldsymbol{V}_n (n = 1, \ldots, N)$. $\mathcal{G}$ denotes the core tensor which fulfills

$$\mathcal{G} = \mathcal{X} \times_1 \boldsymbol{U}_1^{\mathrm{H}} \times_2 \boldsymbol{U}_2^{\mathrm{H}} \times_3 \cdots \times_N \boldsymbol{U}_N^{\mathrm{H}}. \tag{18}$$

According to Definition 1, the received data model in Eqs. (9) and (10) can be constructed as two new three-order tensors. In order to utilize the noncircular characteristic, we firstly stack the received data and it conjugate accoding to mode-1 unfolding and mode-2 unfolding of a three order tensor. Then, we rearrange two new extended three-order tensors by concatening the unfolding data along the mode-1 and mode-2, respectively.

3.2. Tensor-based noncircular signal subspace estimation

Accodring to Eqs. (9) and (10), the two new tensor models can be defined as follows:

$$\mathcal{Y}^{\mathrm{nc}} = \mathcal{A}^{\mathrm{nc}} \times_3 \mathcal{S}^{\mathrm{T}} + \mathcal{N}^{\mathrm{nc}}, \tag{19}$$

$$\tilde{\mathcal{Y}}^{\mathrm{nc}} = \mathcal{B}^{\mathrm{nc}} \times_3 \mathcal{S}^{\mathrm{T}} + \tilde{\mathcal{N}}^{\mathrm{nc}}, \tag{20}$$

where

$$\mathcal{A}^{\rm nc} = [\boldsymbol{A}_{\rm nc1}(:,1) \sqcup_3 \boldsymbol{A}_{\rm nc1}(:,2) \sqcup_3 \cdots \boldsymbol{A}_{\rm nc1}(:,K)] \in \mathbb{C}^{2M_2\times M_2\times K}, \tag{21}$$

$$\mathcal{B}^{\rm nc} = [\boldsymbol{B}_{\rm nc1}(:,1) \sqcup_3 \boldsymbol{B}_{\rm nc1}(:,2) \sqcup_3 \cdots \boldsymbol{B}_{\rm nc1}(:,K)] \in \mathbb{C}^{2M_2\times M_2\times K}, \tag{22}$$

where $\sqcup$ denotes the concatenation of along the 3rd mode of $\mathcal{A}^{\rm nc}$ or $\mathcal{B}^{\rm nc}$, respectively. From Eq. (19), we can find that the noncircular property can double the number of elements corresponding to DOD. According to Definition 3, the multi-SVD of $\mathcal{Y}^{\rm nc}$ can be expressed as

$$\mathcal{Y}^{\rm nc} = \mathcal{S}^{\rm nc} \times_1 U_1^{\rm nc} \times_2 U_2^{\rm nc} \times_3 U_3^{\rm nc}, \tag{23}$$

where $U_i^{\rm nc}$ $(i=1,2,3)$ is the left singular vectors of the i-mode matrix unfolding of $\mathcal{Y}^{\rm nc}$, and $\mathcal{S}^{\rm nc}$ denotes the corresponding core tensor. Then, the signal subspace tensor can be denoted as

$$\mathcal{U}_s^{\rm nc} = \mathcal{S}_s^{\rm nc} \times_1 U_{1s}^{\rm nc} \times_2 U_{2s}^{\rm nc}, \tag{24}$$

where $U_{is}^{\rm nc}$ contains the column vectors of $U_i^{\rm nc}$ corresponding to the K largest singular values;

$$\mathcal{S}_s^{\rm nc} = \mathcal{Y}^{\rm nc} \times_1 (U_{1s}^{\rm nc})^H \times_2 (U_{2s}^{\rm nc})^H \times_3 (U_{3s}^{\rm nc})^H$$

stands for the signal component of $\mathcal{S}^{\rm nc}$. By substituting $\mathcal{S}_s^{\rm nc}$ into Eq. (24) yields

$$\mathcal{U}_s^{\rm nc} = \mathcal{Y}^{\rm nc} \times_1 [U_{1s}^{\rm nc}(U_{1s}^{\rm nc})^{\rm H}] \times_2 [U_{2s}^{\rm nc}(U_{2s}^{\rm nc})^{\rm H}] \times_3 (U_{3s}^{\rm nc})^{\rm H}. \tag{25}$$

Thus, the extend signal subspace matrix $U_s^{\rm nc}$ corresponding to DOD can be obtained

$$U_s^{\rm nc} = [\mathcal{U}_s^{\rm nc}]_{(3)}^{\rm T} = [(U_{1s}^{\rm nc}(U_{1s}^{\rm nc})^{\rm H}) \otimes (U_{2s}^{\rm nc}(U_{2s}^{\rm nc})^{\rm H})]\boldsymbol{Y}_{1nc}(U_{3s}^{\rm nc})^*. \tag{26}$$

As $U_s^{\rm nc}$ and $\boldsymbol{A}_{\rm nc1}$ span the same column space, there is a non-singular matrix $\boldsymbol{H}$ that satisfies

$$U_s^{\rm nc} = \boldsymbol{A}_{\rm nc1}\boldsymbol{H}. \tag{27}$$

Define two selection matrix as follows:

$$\begin{cases} H_1^{\rm nc} = \begin{bmatrix} 1 & 0 \\ 0 & 1 \end{bmatrix} \otimes H_1, \\ H_2^{\rm nc} = \begin{bmatrix} 1 & 0 \\ 0 & 1 \end{bmatrix} \otimes H_2, \end{cases} \tag{28}$$

where

$$H_1 = \begin{bmatrix} I_{M_2-1} & 0_{(M_2-1)\times 1} \end{bmatrix} \otimes I_{M_2}, \tag{29}$$

$$H_2 = \begin{bmatrix} 0_{(M_2-1)\times 1} & I_{M_2-1} \end{bmatrix} \otimes I_{M_2}. \tag{30}$$

Thus, by utilizing the rotational invariance property inherented in $\boldsymbol{A}_{\rm nc1}$, we can obtain

$$\begin{aligned} & H_2^{\rm nc}\boldsymbol{A}_{\rm nc1} = H_1^{\rm nc}\boldsymbol{A}_{\rm nc1}\boldsymbol{\Psi}_{\rm nc} \\ \Leftrightarrow\ & H_2^{\rm nc}U_s^{\rm nc}\boldsymbol{H}^{-1} = H_1^{\rm nc}U_s^{\rm nc}\boldsymbol{H}^{-1}\boldsymbol{\Psi}_{\rm nc} \\ \Leftrightarrow\ & \boldsymbol{H}^{-1}\boldsymbol{\Psi}_{\rm nc}\boldsymbol{H} = (H_1^{\rm nc}U_s^{\rm nc})^{\dagger}H_2^{\rm nc}U_s^{\rm nc} \\ \Leftrightarrow\ & \boldsymbol{\Psi}_{1nc} = (H_1^{\rm nc}U_s^{\rm nc})^{\dagger}H_2^{\rm nc}U_s^{\rm nc}, \end{aligned} \tag{31}$$

where

$$\boldsymbol{\Psi}_{\rm nc} = {\rm diag}\left[{\rm e}^{{\rm j}\pi M_1\sin(\theta_1)}, {\rm e}^{{\rm j}\pi M_1\sin(\theta_2)}, \ldots, {\rm e}^{{\rm j}\pi M_1\sin(\theta_K)}\right],$$

$\boldsymbol{\Psi}_{\rm 1nc} = \boldsymbol{H}^{-1}\boldsymbol{\Psi}_{\rm nc}\boldsymbol{H}$. By performing eigenvalue decomposition on $\boldsymbol{\Psi}_{\rm 1nc}$, we can obtain

$$\boldsymbol{\Psi}_{\rm 1nc} = \tilde{\boldsymbol{H}}^{-1}\boldsymbol{\Lambda}_{\rm 1nc}\tilde{\boldsymbol{H}}, \tag{32}$$

where $\boldsymbol{\Lambda}_{\rm 1nc} = {\rm diag}[\lambda_{\theta_1}, \lambda_{\theta_2}, \ldots, \lambda_{\theta_K}]$ denotes the eigenvalue matrix. Finally, the estimated DOD $\tilde{\theta}_k$ can be expressed as

$$\tilde{\theta}_k = \arcsin\left(\frac{\arg(\lambda_{\theta_k})}{\pi M_1}\right), \quad k = 1,2,\ldots,K. \tag{33}$$

Then, in order to estimate the DOA $\tilde{\phi}_k$, $k=1,2,\ldots,K$, we perform the multi-SVD on $\tilde{\mathcal{Y}}^{\rm nc}$

$$\tilde{\mathcal{Y}}^{\rm nc} = \tilde{\mathcal{S}}^{\rm nc} \times_1 \tilde{U}_1^{\rm nc} \times_2 \tilde{U}_2^{\rm nc} \times_3 \tilde{U}_3^{\rm nc}, \tag{34}$$

where $\tilde{U}_i^{\rm nc}$ $(i=1,2,3)$ is the left singular vectors of the i-mode matrix unfolding of $\tilde{\mathcal{Y}}^{\rm nc}$, and $\tilde{\mathcal{S}}^{\rm nc}$ denotes the corresponding core tensor. Then, the signal subspace tensor can be denoted as

$$\tilde{\mathcal{U}}_s^{\rm nc} = \tilde{\mathcal{S}}_s^{\rm nc} \times_1 \tilde{U}_{1s}^{\rm nc} \times_2 \tilde{U}_{2s}^{\rm nc}, \tag{35}$$

where $\tilde{U}_{is}^{\rm nc}$ contains the column vectors of $\tilde{U}_i^{\rm nc}$ corresponding to the K largest singular values;

$$\tilde{\mathcal{S}}_s^{\rm nc} = \tilde{\mathcal{Y}}^{\rm nc} \times_1 (\tilde{U}_{1s}^{\rm nc})^{\rm H} \times_2 (\tilde{U}_{2s}^{\rm nc}))^{\rm H} \times_3 (\tilde{U}_{3s}^{\rm nc})^{\rm H}$$

stands for the signal component of $\tilde{\mathcal{S}}^{\rm nc}$. By substituting $\tilde{\mathcal{S}}_s^{\rm nc}$ into Eq. (35) yields

$$\tilde{\mathcal{U}}_s^{\rm nc} = \tilde{\mathcal{Y}}^{\rm nc} \times_1 [\tilde{U}_{1s}^{\rm nc}(\tilde{U}_{1s}^{\rm nc})^H] \times_2 [\tilde{U}_{2s}^{\rm nc}(\tilde{U}_{2s}^{\rm nc})^{\rm H}] \times_3 (\tilde{U}_{3s}^{\rm nc})^{\rm H}. \tag{36}$$

Thus, the extend signal subspace matrix $\tilde{U}_s^{\rm nc}$ corresponding to DOD can be obtained

$$\tilde{U}_s^{\rm nc} = [\tilde{\mathcal{U}}_s^{\rm nc}]_{(3)}^{\rm T} = [\tilde{U}_{1s}^{\rm nc}(\tilde{U}_{1s}^{\rm nc})^{\rm H}) \otimes (\tilde{U}_{2s}^{\rm nc}(\tilde{U}_{2s}^{\rm nc})^{\rm H})]\boldsymbol{Y}_{2nc}(\tilde{U}_{3s}^{\rm nc})^*. \tag{37}$$

Due to that $\tilde{U}_s^{\rm nc}$ and $U_s^{\rm nc}$ span the same column space, thus

$$\tilde{U}_s^{\rm nc} = \boldsymbol{T}U_s^{\rm nc}. \tag{38}$$

Insertation $U_s^{\rm nc} = \boldsymbol{A}_{\rm nc1}\boldsymbol{H}$ into Eq. (38), we can obtain

$$\tilde{U}_s^{\rm nc} = \boldsymbol{T}\boldsymbol{A}_{\rm nc1}\boldsymbol{H} = \boldsymbol{B}_{\rm nc1}\boldsymbol{H}. \tag{39}$$

According to the selection matrices in Eq. (28), the rotational relationship for DOA can be constructed as

$$H_2^{\rm nc}\boldsymbol{B}_{\rm nc1} = H_1^{\rm nc}\boldsymbol{B}_{\rm nc1}\boldsymbol{\Phi}_{\rm nc}$$

$$\Leftrightarrow H_2^{\rm nc}\tilde{U}_s^{\rm nc}\boldsymbol{H}^{-1}=H_1^{\rm nc}\tilde{U}_s^{\rm nc}\boldsymbol{H}^{-1}\boldsymbol{\Phi}_{\rm nc}$$
$$\Leftrightarrow \boldsymbol{H}^{-1}\boldsymbol{\Phi}_{\rm nc}\boldsymbol{H}=(H_1^{\rm nc}\tilde{U}_s^{\rm nc})^{\dagger}H_2^{\rm nc}\tilde{U}_s^{\rm nc}$$
$$\Leftrightarrow \boldsymbol{\Phi}_{\rm 1nc}=(H_1^{\rm nc}\tilde{U}_s^{\rm nc})^{\dagger}H_2^{\rm nc}\tilde{U}_s^{\rm nc}, \tag{40}$$

where

$$\boldsymbol{\Phi}_{\rm nc}=\mathrm{diag}\left[\mathrm{e}^{\mathrm{j}\pi M_1\sin(\phi_1)},\mathrm{e}^{\mathrm{j}\pi M_1\sin(\phi_2)},\ldots,\mathrm{e}^{\mathrm{j}\pi M_1\sin(\phi_K)}\right],$$
$$\boldsymbol{\Phi}_{\rm 1nc}=\boldsymbol{H}^{-1}\boldsymbol{\Phi}_{\rm nc}\boldsymbol{H}.$$

From Eqs. (31), (32), and (40), we can find that the eigenvectors corresponding to DOD and DOA are the same, thus, the estimated DODs and DOAs are automatically paired. Thus, the estimated $\tilde{\boldsymbol{\Phi}}_{\rm nc}$ can be obtained as

$$\tilde{\boldsymbol{\Phi}}_{\rm nc}=\tilde{\boldsymbol{H}}\boldsymbol{\Phi}_{\rm 1nc}\tilde{\boldsymbol{H}}^{-1}, \tag{41}$$

where $\tilde{\boldsymbol{\Phi}}_{\rm nc}=\mathrm{diag}[\lambda_{\phi_1},\lambda_{\phi_2},\ldots,\lambda_{\phi_K}]$ denotes the eigenvalue matrix corresponding to $\boldsymbol{\Phi}_{\rm 1nc}$. Thus, the estimated DOA $\tilde{\phi}_k$ can be expressed as

$$\tilde{\phi}_k=\arcsin\left(\frac{\arg(\lambda_{\phi_k})}{\pi M_1}\right),\quad k=1,2,\ldots,K. \tag{42}$$

It is easily to show that by using the non-circular characteristic of the imping sources, the virtual aperture of coprime MIMO radar can be enhanced and the extend tensor model corresponding to DOD and DOA can make full use of the multidimensional structure information inherented in the received data. From Eqs. (33) and (42), the ambiguous DODs and DOAs exist due to inter-element spacing is larger than half wavelength. Thus, in the following analyses, we will demonstrate that all the ambiguous angles can be located and the true angle can be estimated with the aid of the coprime property.

3.3. Ambiguity elimination

Assume that the DOD and DOA of a single noncircular target are (θ,ϕ), the phase differences for DOD and DOA in the coprime MIMO radar can be respectively denoted as

$$\begin{cases}\Delta_\theta=\mathrm{mod}(\pi M_i\sin(\theta),2\pi),\\ \Delta_\phi=\mathrm{mod}(\pi M_i\sin(\phi),2\pi).\end{cases} \tag{43}$$

Due to the phase periodicity of complex exponential function is 2π, thus the phase differences for DOD and DOA can be redenoted as

$$\begin{cases}\Delta_\theta+2k_\theta\pi=\pi M_i\sin(\theta),\\ \Delta_\phi+2k_\phi\pi=\pi M_i\sin(\phi),\end{cases} \tag{44}$$

where k_θ and k_ϕ are integers. Since

$$\theta,\phi\in[-\pi/2,\pi/2],$$
$$k_\theta\in[-M_i/2-\Delta_\theta/2\pi,M_i/2-\Delta_\theta/2\pi],$$
$$k_\phi\in[-M_i/2-\Delta_\phi/2\pi,M_i/2-\Delta_\phi/2\pi].$$

So, the phase relationship between the actual and ambiguous can be denoted as

$$\sin(\theta)-\sin(\theta_a)=\frac{2k_\theta}{M_i},$$
$$\sin(\phi)-\sin(\phi_a)=\frac{2k_\phi}{M_i}, \tag{45}$$

where θ_a and ϕ_a denote the ambiguous DOD and DOA, respectively. For coprime MIMO radar, the inter-element spacing of the first sparse subarray and the second sparse subarray satisfy the coprime property, thus the actual DOD and DOA can be obtained. According to Eq. (45), the phase relationship between the actual and ambiguous for the first subarray and the second subarray can be further denoted as

$$\begin{cases}\sin(\theta)-\sin(\theta_{a1})=\dfrac{2k_{\theta1}}{M_1},\\ \sin(\phi)-\sin(\phi_{a1})=\dfrac{2k_{\phi1}}{M_1},\end{cases}$$
$$\begin{cases}\sin(\theta)-\sin(\theta_{a2})=\dfrac{2k_{\theta2}}{M_2},\\ \sin(\phi)-\sin(\phi_{a2})=\dfrac{2k_{\phi2}}{M_2}.\end{cases} \tag{46}$$

Then, by using the coprime property, the true DOD and DOA satisfy

$$\frac{k_{\theta1}}{M_1}=\frac{k_{\theta2}}{M_2}\quad\text{and}\quad\frac{k_{\phi1}}{M_1}=\frac{k_{\phi2}}{M_2}. \tag{47}$$

As M_1 and M_2 satisfies the coprime property, $\{k_{\theta1},k_{\theta2}\}$ and $\{k_{\phi1},k_{\phi2}\}$ are unique that satisfy Eq. (46), except for $k_{\theta1}=k_{\theta2}=0$ and $k_{\phi1}=k_{\phi2}=0$. Thus, the estimated actual DOD and DOA corresponding to the theoretical DOD and DOA can be obtained by finding the common angle. But, due to the effect of noise, the estimated true DOD and DOA by the first subarray and the second subarray cannot be perfect concidences. Thus, the estimated actual DOD and DOA can be obtained by using the method in Ref. [30].

After obtaining the estimated $(\sin(\theta_{a1}),\sin(\phi_{a1}))$, $(\sin(\theta_{a2}),\sin(\phi_{a2}))$ for the first subarray and the second subarray, the finally true DOD and DOA can be denoted as

$$\tilde{\theta}=\arcsin\left(\frac{\sin(\theta_{a1})+\sin(\theta_{a2})}{2}\right),$$
$$\tilde{\phi}=\arcsin\left(\frac{\sin(\phi_{a1})+\sin(\phi_{a2})}{2}\right). \tag{48}$$

And, for K targets, the actual DODs and DOAs with (θ_k,ϕ_k) for $k=1,2,\ldots,K$ can be achieved by using the above mentioned ambiguity elimination process.

In order to make our proposed method more comprehensive, the main steps of our scheme for angle estimation in coprime MIMO radar is summarized in Algorithm 1.

Algorithm 1 Summary of the proposed method

Input: array received data $\boldsymbol{Y}_{1\mathrm{nc}}, \boldsymbol{Y}_{2nc}$ for the first subarray of the coprime MIMO radar
Output: unambiguous estimated true DODs $\tilde{\theta}_k$ and DOAs $\tilde{\phi}_k$ for $k = 1,2,\ldots,K$

Step 1 Construct two new extend three-order tensor for noncircular sources according to Eqs. (19) and (20).
Step 2 Perform multi-SVD on $\mathcal{Y}^{\mathrm{nc}}$ and $\tilde{\mathcal{Y}}^{\mathrm{nc}}$ to get U_i^{nc} and $\tilde{U}_i^{\mathrm{nc}}$ $(i = 1,2,3)$ via Eqs. (23) and (34).
Step 3 Construct the extend signal subspace matrix U_s^{nc} for DOD and $\tilde{U}_s^{\mathrm{nc}}$ for DOA according to Eqs. (26) and (37).
Step 4 Obtain $\boldsymbol{\Psi}_{1\mathrm{nc}}$ and $\boldsymbol{\Phi}_{1\mathrm{nc}}$ by using the rotational invariance relationship according to Eqs. (31) and (40) with the help of selection matrix H_1^{nc} and H_2^{nc} in Eq. (28).
Step 5 Calculate the automatically paired DODs $\tilde{\theta}_k = \arcsin(\arg(\lambda_{\theta_k})/\pi M_1)$ and DOAs $\tilde{\phi}_k = \arcsin(\arg(\lambda_{\phi_k})/\pi M_1)$ for $k = 1,2,\ldots,K$ according to Eqs. (33) and (42) due to the utilization of the same eigenvector matrix.
Step 6 Repeat Step 1 to Step 5 to obtain the automatically paired DODs and DOAs by using the second sparse subarray received data of the coprime MIMO radar.
Step 7 Calculate all the ambiguous DODs and DOAs via Eq. (46) for the first subarray and the second subarray in the coprime MIMO radar and search for the nearest ones by using the coprime property.
Step 8 Obtain the unambiguous true DODs $\tilde{\theta}_k = \arcsin(\sin(\theta_{ak1}) + \sin(\theta_{ak2})/2)$ and DOAs $\tilde{\phi}_k = \arcsin(\sin(\phi_{ak1}) + \sin(\phi_{ak2})/2)$ according to Eq. (48).

4. Performance analysis

4.1. Complexity analysis

For coprime MIMO radar, the computational complexity of the proposed method mainly contains multi-SVD for extend three-order noncircular tensors $\mathcal{Y}^{\mathrm{nc}}$ and $\tilde{\mathcal{Y}}^{\mathrm{nc}}$, computes the signal subspace matrices $\tilde{U}_s^{\mathrm{nc}}$ and U_s^{nc}, and constructs the rotational invariance relationship for DOD and DOA. Thus, the total computational complexity of the proposed method is $\mathcal{O}(16(M_1^2 + M_2^2)LK + 10(M_1^2 + M_2^2)K + 16(M_1^6 + M_2^6) + 8(M_1^4 + M_2^4)L + 8(M_1^3(M_1 - 1) + M_2^3(M_2 - 1))K + 12K^2(M_2(M_2 - 1) + M_1(M_1 - 1)) + 4K^3)$. The computational loads of RD PSS method in Ref. [30], PARAFAC method in Ref. [31], and ESPRIT method are also summarized for comparison in Table 1. And, l_i $(i = 1,2)$ denotes the times of the partial search with $(0, 2/M_i)$ $(i = 1,2)$; $\boldsymbol{\kappa}$ denotes the interation times of the PARAFAC algorithm.

Table 1. Comparison of the complexity.

Method	Complexity
RD PSS	$\mathcal{O}((M_1^4 + M_2^4)L + M_1^6 + M_2^6 + l_2 M_2^3\ (M_2^2 - K + 1) + l_1 M_1^3 (M_1^2 - K + 1))$
PARAFAC	$\mathcal{O}(\boldsymbol{\kappa}(6K^3 + 3KL(M_1^2 + M_2^2) + 3K^2\ (M_1^2 + M_2^2 + 2(M_1 + M_2)L)))$
ESPRIT	$\mathcal{O}(L(M_1^4 + M_2^4) + M_1^6 + M_2^6 + 2K^2\ (M_1(M_1 - 1) + M_2(M_2 - 1)) + 2K^2\ (M_1 + M_2 - 2) + 12K^3)$
Proposed	$\mathcal{O}((16(M_1^2 + M_2^2)LK + 10(M_1^2 + M_2^2)K + 16(M_1^6 + M_2^6) + 8(M_1^4 + M_2^4)L + 8(M_1^3(M_1 - 1) + M_2^3(M_2 - 1))K + 12K^2(M_2(M_2 - 1) + M_1(M_1 - 1)) + 4K^3))$

In order to provide an intuitive computational complexity comparison, the complexity *versus* different arrays and snapshots are demonstrated in Fig. 2 and Fig. 3. In Fig. 2, the number of the second sparse subarray increases from 3 to 9 with a step of 2 and the first sparse subarray is fixed at 4. In Fig. 3, the number of snapshots ranges from 100 to 1000 with a step of 100 and the first sparse subarray and the second sparse subarray is 4 and 5, respectively. Both in Fig. 2 and Fig. 3, the partial search interval used in the RD PSS method is set to 0.01 and the interation times of the PARAFAC algorithm is 200. As shown in Fig. 2 and Fig. 3, the computational load of the proposed method is relatively high among all the methods due to the multi-SVD operation. But it can provide better angle estimation performance, which can be verified in Section 5.

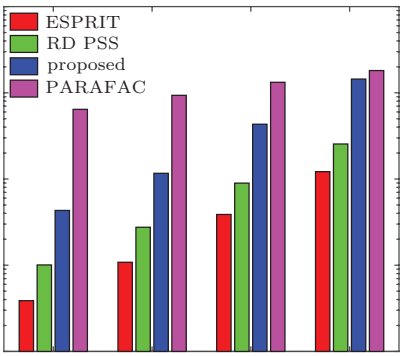


Fig. 2. Comparison of the computational complexity with different M_2.

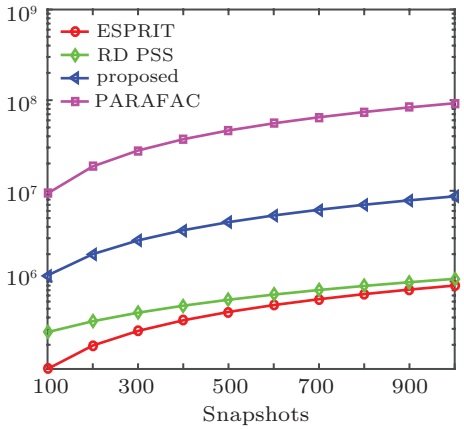


Fig. 3. Comparison of the computational complexity with different snapshots.

4.2. Identified targets

According to Eqs. (24) and (35), the maximum number of sources that can be resolved by using the proposed method is $\min(M_1-1, M_2-1)$. Although, the multi-SVD method cannot improve the degrees of freedom, the estimated signal subspace matrices in Eqs. (26) and (37) by exploiting the multi-dimensional structure inherent in the received signal can restrain the effect of noise effectively compared with traditional subspace-based methods. Thus, the proposed method with the aid of the noncircular property mainly focus on the improvement in estimation accuracy.

4.3. CRB

In order to provide a benchmark for parameter estimation performance, we derive the closed-form expression of the deterministic CRB for noncircular sources in bistatic coprime MIMO radar. Firstly, we stack all the array output of the first sparse subarray and the second sparse subarray as follows:

$$\tilde{\boldsymbol{Y}}_{\text{sum}} = \begin{bmatrix} \boldsymbol{A}_{\text{nc1}} \\ \boldsymbol{A}_{\text{nc2}} \end{bmatrix} \boldsymbol{S}_0 + \tilde{\boldsymbol{N}}_{\text{nc}}, \tag{49}$$

where $\boldsymbol{A}_{\text{nc1}}$ and $\boldsymbol{A}_{\text{nc2}}$ denote the extend noncircular steering matrix corresponding to the first and second subarrays in coprime MIMO radar, respectively. And, $\boldsymbol{A}_{\text{nc2}}$ has the similar form as the $\boldsymbol{A}_{\text{nc1}}$, which can be expressed as

$$\boldsymbol{A}_{\text{nc2}} = \begin{bmatrix} (\boldsymbol{A}_2(\theta)\boldsymbol{\Xi}) \odot \boldsymbol{B}_2(\phi) \\ (\boldsymbol{A}_2(\theta)\boldsymbol{\Psi}_2\boldsymbol{\Phi}_2\boldsymbol{\Xi}_1) \odot \boldsymbol{B}_2(\phi) \end{bmatrix}, \tag{50}$$

where

$$\boldsymbol{\Psi}_2 = \text{diag}[\text{e}^{\text{j}\pi M_1(M_2-1)\sin(\theta_1)}, \text{e}^{\text{j}\pi M_1(M_2-1)\sin(\theta_2)}, \ldots, \text{e}^{\text{j}\pi M_1(M_2-1)\sin(\theta_K)}],$$
$$\boldsymbol{\Phi}_2 = \text{diag}[\text{e}^{\text{j}\pi M_1(M_2-1)\sin(\phi_1)}, \text{e}^{\text{j}\pi M_1(M_2-1)\sin(\phi_2)}, \ldots, \text{e}^{\text{j}\pi M_2(M_1-1)\sin(\phi_K)}],$$

$\boldsymbol{A}_2 = [\boldsymbol{a}_2(\theta_1), \boldsymbol{a}_2(\theta_2), \ldots, \boldsymbol{a}_2(\theta_K)] \in \mathbb{C}^{M_1 \times K}$, and $\boldsymbol{B}_2 = [\boldsymbol{b}_2(\phi_1), \boldsymbol{b}_2(\phi_2), \ldots, \boldsymbol{b}_2(\phi_K)] \in \mathbb{C}^{M_1 \times K}$ is the steering matrix according to the second subarray of coprime array in both transmit and receive side. The direction steering vectors $\boldsymbol{a}_2(\theta_k)$ and $\boldsymbol{b}_2(\theta_k)$ satisfy

$$\boldsymbol{a}_2(\theta_k) = [1, \text{e}^{-\text{j}\pi M_2 \sin(\theta_k)}, \ldots, \text{e}^{-\text{j}\pi M_2(M_1-1)\sin(\theta_k)}]^{\text{T}}, \tag{51}$$
$$\boldsymbol{b}_2(\theta_k) = [1, \text{e}^{-\text{j}\pi M_2 \sin(\phi_k)}, \ldots, \text{e}^{-\text{j}\pi M_2(M_1-1)\sin(\phi_k)}]^{\text{T}}. \tag{52}$$

The estimated parameters can be written as the vector form

$$\begin{cases} \boldsymbol{\theta} = [\theta_1, \theta_2, \ldots, \theta_K], \\ \boldsymbol{\phi} = [\phi_1, \phi_2, \ldots, \phi_K]. \end{cases} \tag{53}$$

Define the total steering matrix as follows:

$$\boldsymbol{A}_{sum} = \begin{bmatrix} \boldsymbol{A}_{\text{nc1}} \\ \boldsymbol{A}_{\text{nc2}} \end{bmatrix} = \begin{bmatrix} (\boldsymbol{A}_1(\theta)\boldsymbol{\Xi}) \odot \boldsymbol{B}_1(\phi) \\ (\boldsymbol{A}_1(\theta)\boldsymbol{\Psi}_1\boldsymbol{\Phi}_1\boldsymbol{\Xi}_1) \odot \boldsymbol{B}_1(\phi) \\ (\boldsymbol{A}_2(\theta)\boldsymbol{\Xi}) \odot \boldsymbol{B}_2(\phi) \\ (\boldsymbol{A}_2(\theta)\boldsymbol{\Psi}_2\boldsymbol{\Phi}_2\boldsymbol{\Xi}_1) \odot \boldsymbol{B}_2(\phi) \end{bmatrix}. \tag{54}$$

According to Ref. [35], the CRB matrix can be represented by

$$\textbf{CRB}_{\text{nc}} = \frac{\sigma^2}{2L}\left\{\text{Re}[\boldsymbol{D}_{\text{sum}}^{\text{H}}\boldsymbol{\Pi}_{\boldsymbol{A}_{\text{sum}}}^{\perp}\boldsymbol{D}_{\text{sum}} \oplus \boldsymbol{R}_{ss}]\right\}^{-1}, \tag{55}$$

where $\boldsymbol{\Pi}_{\boldsymbol{A}_{\text{sum}}}^{\perp} = \boldsymbol{I}_{2M_2^2+2M_1^2} - \boldsymbol{A}_{\text{sum}}(\boldsymbol{A}_{\text{sum}}^{\text{H}}\boldsymbol{A}_{\text{sum}})^{-1}\boldsymbol{A}_{\text{sum}}^{\text{H}}$ denotes the project matrix; $\boldsymbol{R}_{ss}$ denotes the signal covariance matrix, which can be expressed as

$$\boldsymbol{R}_{ss} = \begin{bmatrix} \boldsymbol{S}_0\boldsymbol{S}_0^{\text{H}}/L & \boldsymbol{S}_0\boldsymbol{S}_0^{\text{H}}/L \\ \boldsymbol{S}_0\boldsymbol{S}_0^{\text{H}}/L & \boldsymbol{S}_0\boldsymbol{S}_0^{\text{H}}/L \end{bmatrix} \tag{56}$$

and $\boldsymbol{D}_{\text{sum}} = \left[\partial\boldsymbol{A}_{\text{sum}}/\partial\boldsymbol{\theta} \;\; \partial\boldsymbol{A}_{\text{sum}}/\partial\boldsymbol{\phi}\right]$ denotes the partial derivative matrix corresponding to DODs and DOAs, the detailed expression for $\left[\partial\boldsymbol{A}_{\text{sum}}/\partial\boldsymbol{\theta} \;\; \partial\boldsymbol{A}_{\text{sum}}/\partial\boldsymbol{\phi}\right]$ can be denoted as follows:

$$\frac{\partial\boldsymbol{A}_{\text{sum}}}{\partial\boldsymbol{\theta}} = \begin{bmatrix} \dfrac{\partial\boldsymbol{A}_1(\theta)}{\partial\boldsymbol{\theta}}\boldsymbol{\Xi} \odot \boldsymbol{B}_1(\phi) \\ \left(\dfrac{\partial\boldsymbol{A}_1(\theta)}{\partial\boldsymbol{\theta}}(\theta)\boldsymbol{\Psi}_1\boldsymbol{\Phi}_1\boldsymbol{\Xi}_1 + \boldsymbol{A}_1(\theta)\dfrac{\partial\boldsymbol{\Psi}_1}{\partial\boldsymbol{\theta}}\boldsymbol{\Phi}_1\boldsymbol{\Xi}_1\right) \odot \boldsymbol{B}_1(\phi) \\ \dfrac{\partial\boldsymbol{A}_2(\theta)}{\partial\boldsymbol{\theta}}\boldsymbol{\Xi} \odot \boldsymbol{B}_2(\phi) \\ \left(\dfrac{\partial\boldsymbol{A}_2(\theta)}{\partial\boldsymbol{\theta}}(\theta)\boldsymbol{\Psi}_2\boldsymbol{\Phi}_2\boldsymbol{\Xi}_1 + \boldsymbol{A}_2(\theta)\dfrac{\partial\boldsymbol{\Psi}_2}{\partial\boldsymbol{\theta}}\boldsymbol{\Phi}_2\boldsymbol{\Xi}_1\right) \odot \boldsymbol{B}_{21}(\phi) \end{bmatrix}, \tag{57}$$

$$\frac{\partial \boldsymbol{A}_{\text{sum}}}{\partial \phi}=\begin{bmatrix} \boldsymbol{A}_1(\theta)\boldsymbol{\Xi}\odot\dfrac{\partial \boldsymbol{B}_1(\phi)}{\partial \phi} \\ \left(\boldsymbol{A}_1(\theta)\boldsymbol{\Psi}_1\dfrac{\partial \boldsymbol{\Phi}_1}{\partial \phi}\boldsymbol{\Xi}_1\right)\odot\boldsymbol{B}_1(\phi)+(\boldsymbol{A}_1(\theta)\boldsymbol{\Psi}_1\boldsymbol{\Phi}_1\boldsymbol{\Xi}_1)\odot\dfrac{\partial \boldsymbol{B}_1(\phi)}{\partial \phi} \\ \boldsymbol{A}_2(\theta)\boldsymbol{\Xi}\odot\dfrac{\partial \boldsymbol{B}_2(\phi)}{\partial \phi} \\ \left(\boldsymbol{A}_2(\theta)\boldsymbol{\Psi}_2\dfrac{\partial \boldsymbol{\Phi}_2}{\partial \phi}\boldsymbol{\Xi}_1\right)\odot\boldsymbol{B}_2(\phi)+(\boldsymbol{A}_2(\theta)\boldsymbol{\Psi}_2\boldsymbol{\Phi}_2\boldsymbol{\Xi}_1)\odot\dfrac{\partial \boldsymbol{B}_2(\phi)}{\partial \phi} \end{bmatrix}. \tag{58}$$

Thus, the closed-form expression about the deterministic CRB for noncircular sources in coprime MIMO radar is obtained.

5. Simulation results

In this section, several simulations are carried out to evaluate the effectiveness and superiority of the proposed method. And, the state-of-the-art RD PSS algorithm, PARAFAC algorithm, ESPRIT algorithm, and CRB in Eq. (55) are used to compare with the proposed method. In the following simulation, the coprime bistatic MIMO radar is equiped with $M=M_1+M_2-1$ arrays both in transmitter and receiver, where the number of sensors of the first subarrays is M_2 with inter-element interval being M_1 and the number of sensors of the second subarrays is M_1 with inter-element interval being M_2. For fair comparison, a narrowband bistatic MIMO radar system with M transmit antennas and M receive arrays is also considered, both transmit and receive arrays are half-wavelength inter-element spacing ULAs. Unless explicitly stated, the partial search interval used in the RD PSS method for coprime MIMO radar is set to 0.01 and the iteration times of the PARAFAC algorithm is 200 in the simulations. The average root mean square error is defined as follows to measure the estimation performance

$$\text{RMSE}=\sqrt{\frac{1}{KI}\sum_{i=1}^{I}\left(\left\|\tilde{\theta}_i-\theta\right\|^2+\left\|\tilde{\phi}_i-\phi\right\|^2\right)}, \tag{59}$$

where I denotes the number of the independent Monte Carlo trails. $\tilde{\theta}_i$ and $\tilde{\phi}_i$ denote the estimated angular parameters for θ and ϕ in the i-th trial, respectively. And, the RMSE curves presented in the following simulation are obtained by using $I=500$ independent trials.

In the first experiment, a coprime bistatic MIMO radar system with 8 transmit antennas and 8 receive arrays is considered, where $M_1=4$ and $M_2=5$ both in transmitter and receiver. Assume two equi-powered uncorrelated narrowband noncircular sources located at $(\theta_1,\phi_1)=(10^\circ,20^\circ)$, $(\theta_2,\phi_2)=(30^\circ,40^\circ)$, and noncircular phase $\{\psi_k\}_{k=1}^2=[5^\circ,10^\circ]$. A total of 100 snapshots are used and SNR is set to 0 dB to demonstrate the spatial spectrum estimation performance of the proposed algorithm. The simulation results in Figs. 4(a)–4(d) are obtained with the aid of 100 Monte Carlo trials, where the asterisks with different colors denote the estimated results by different methods and the black circles denote the true angles. As illuminated in Figs. 4(a)–4(d), it can be seen that the estimated DODs and DOAs by utilizing the proposed method are well located and the proposed method can provide a better estimation performance compared with other three methods. Furthermore, in order to make the proposed method more convincing, we also demonstrate the estimated performance under the condition of the maximum number of sources that can be resolved by using the proposed method. According to the analysis in Subsection 4.2, the maximum number of sources that can be resolved is 3 for $M_1=4$ and $M_2=5$ both in transmitter and receiver. In Fig. 4(e), three equi-powered uncorrelated narrowband noncircular sources located at $(\theta_1,\phi_1)=(10^\circ,30^\circ)$, $(\theta_2,\phi_2)=(30^\circ,40^\circ)$, and $(\theta_3,\phi_3)=(50^\circ,65^\circ)$. In Fig. 4(f), three equi-powered uncorrelated narrowband noncircular sources located at $(\theta_1,\phi_1)=(45^\circ,10^\circ)$, $(\theta_2,\phi_2)=(35^\circ,30^\circ)$, and $(\theta_3,\phi_3)=(55^\circ,50^\circ)$. In both Figs. 4(e) and 4(f), the noncircular phase are set to $\{\psi_k\}_{k=1}^3=[5^\circ,10^\circ,15^\circ]$. From Figs. 4(e) and 4(f), we can find that the proposed method can provide a better estimated performance under the condition of the maximum resolved number of sources and the angular parameters are automatically paired.

In the second simulation, the RMSE performance as a function of SNR and snapshots for coprime multiple-input multiple-output radar is considered. Other simulation parameters are same as the first simulation. In Fig. 5(a), the SNR increases from 0 dB to 10 dB with a step of 1 dB and the snapshots is fixed at 100. It is clear that the proposed method by using the noncircular property can provide a high estimation precision from high noise region to low noise region. In Fig. 5(b), the number of snapshots increases from 80 to 1000 with a step of 40 and the SNR is 0 dB for all snapshots. From Fig. 5(b), it can be seen that the angle estimation performance of the proposed algorithm is remarkably enhanced with the number of the snapshots increases and the proposed method still work well when the available snapshots is relatively limited. And, as illuminated in Fig. 5, the coprime transmit and receive array in multiple-input multiple-output radar can enlarge the virtual array aperture. Therefore, the larger inter-element spacing array will provide a higher estimation performance compared with that of half-wavelength spacing bistatic multiple-input multiple-output radar. Moreover, it can be ob-

served that the noncircular property can further enhance the virtual array aperture to improve the estimation performance. So, the proposed method can exhibit excellent performance for different snapshots and SNRs.

In the third simulation, the RMSE performance comparison *versus* different numbers of transmit and receive arrays in bistatic coprime MIMO radar is investigated. Two types of coprime MIMO radar with $(M_1, M_2) = (4, 5)$ and $(M_1, M_2) = (3, 4)$ are adopted. The number of imping sources, the range of snapshots, and SNR are the same as those as the second simulation. As shown in Fig. 6, we can find that the estimated performance for all methods increase with the number of transmit and receive arrays increasing. And, the proposed method are superior to other methods in the condition of different types of transmit and receive arrays for coprime MIMO radar, which demonstrate that the constructed tensor-based noncircular signal model is efficient to improve the estimation performance.

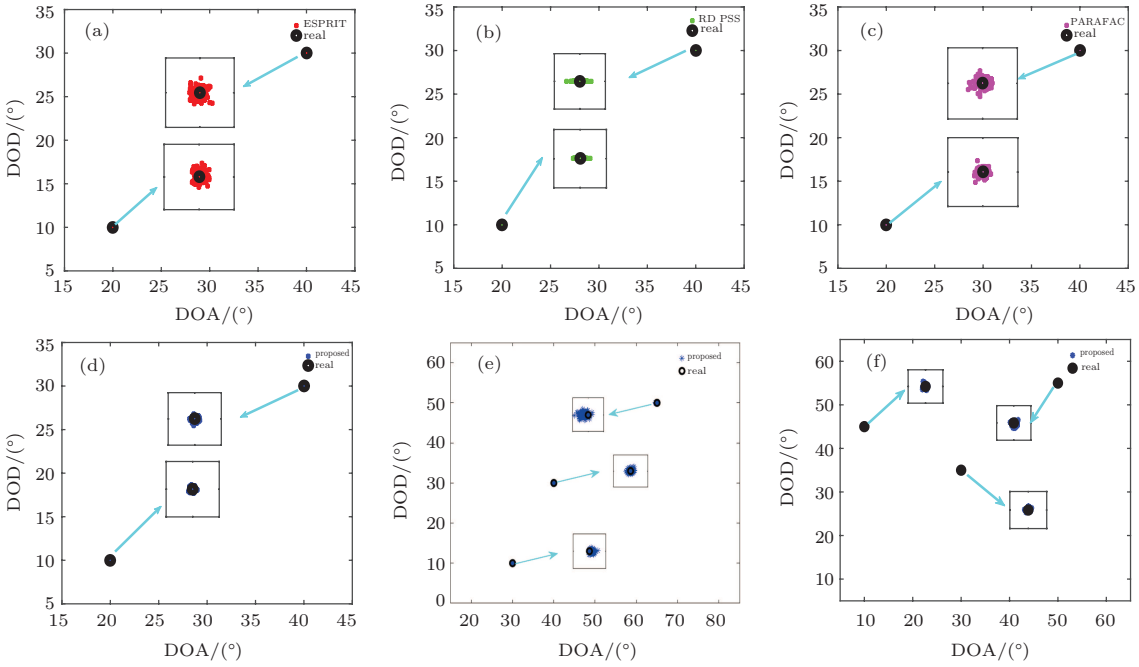


Fig. 4. Scatter comparison of different methods with snapshots = 100 and SNR = 0 dB. (a) Scatter plot of the ESPRIT method. (b) Scatter plot of the RD PSS method.(c) Scatter plot of the PARAFAC method.(d) Scatter plot of the proposed method. (e) Scatter plot of the proposed method for three targets. (f) Scatter plot of the proposed method for three targets.

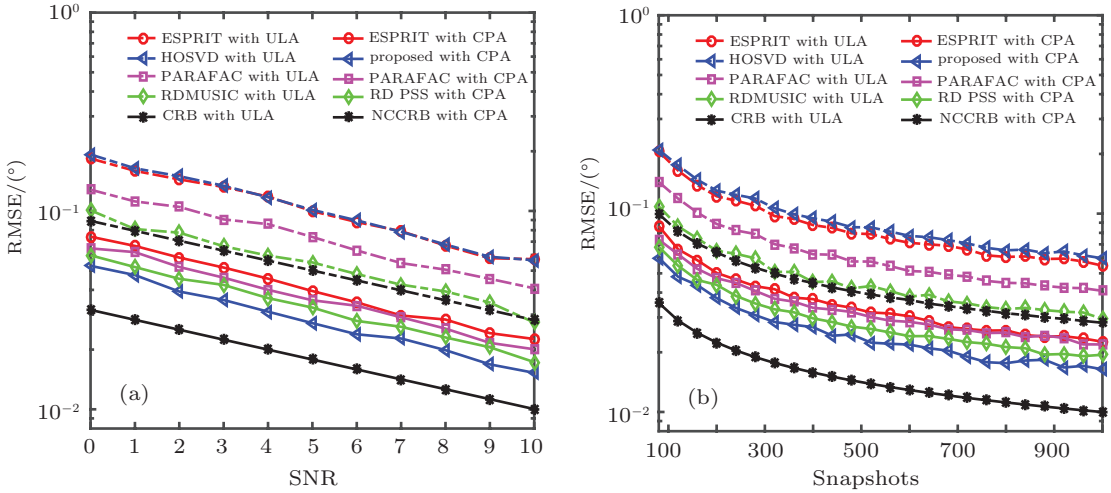


Fig. 5. RMSE performance *versus* SNR and snapshots: (a) RMSE *versus* SNR with snapshots = 100 and (b) RMSE *versus* snapshots with SNR = 0 dB.

In the last experiment, we compare the angular super-resolution capabilities of the above mentioned algorithms. Two closely targets are considered, the DOD and DOA of the first target are $(\theta_1, \phi_1) = (10°, 20°)$ and the DOD and DOA of the second target are $(\theta_2, \phi_2) = (10° + \Delta, 20° + \Delta)$, where Δ varies from 1° to 10° with a step size 1°.

In Figs. 7(a) and 7(b), the SNR is set to be 0 dB, while the number of snapshots are fixed at 100 and 200, respectively. The noncircular phase are the same as the first simulation. As shown in Fig. 7, all methods perform well when the angular

interval is large. when angular interval $\Delta \leq 3°$, the RMSE performance of other three mentioned methods are very poor. But, the proposed method can still guarantee satisfied performance for closely-spaced targets. For a more intuitive comparison, the spatial spectrum estimations for coprime MIMO radar are also provided when the angular separation is small. Consider two closely spaced targets with DODs and DOAs $(\theta_1, \phi_1) = (10°, 20°)$ and $(\theta_2, \phi_2) = (12°, 22°)$, respectively. In Fig. 8, the SNR and snapshots are set to be 0 dB and 100, respectively. Other simulation parameters are the same as Fig. 7. As illuminated in Fig. 8, the scattergram simulation results are obtained with the aid of 100 Monte Carlo trials. It is clear that spatial spectrum estimation of the two closely spaced sources by using the proposed method is relatively more concentrated compared with that of other methods in Figs. 8(a)–8(c). Thus, the simulation results in Figs. 7 and 8 demonstrate that the estimation performance for closely spaced targets by using proposed method is the best.

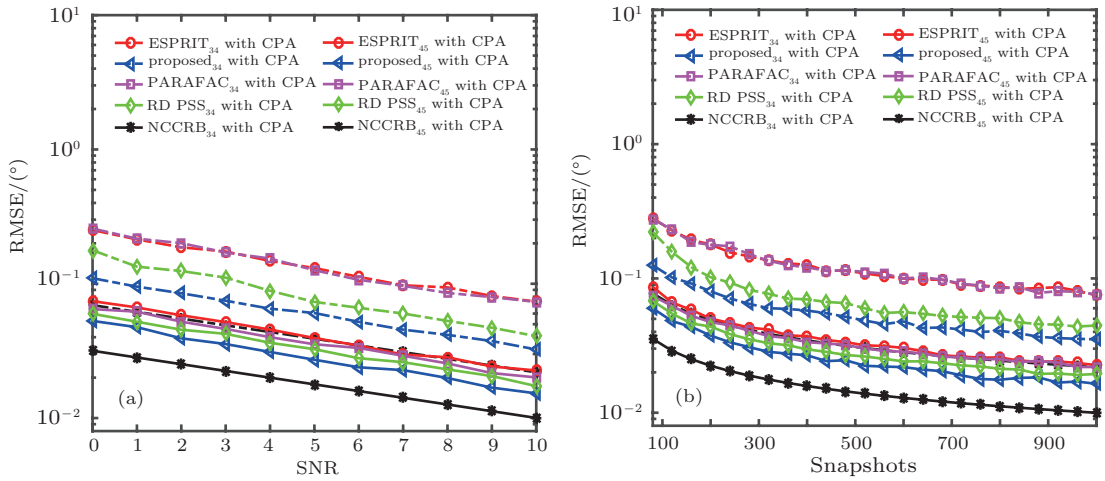


Fig. 6. RMSE performance *versus* different numbers of sensors: (a) RMSE *versus* SNR with snapshots = 100 and (b) RMSE *versus* snapshots with SNR = 0 dB.

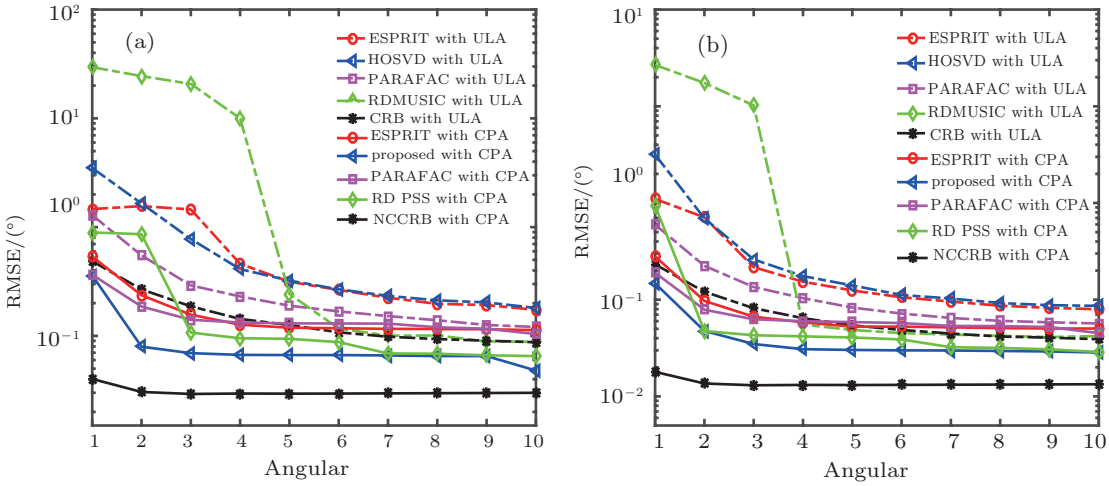


Fig. 7. RMSE *versus* different angle separations with 2 targets: (a) RMSE *versus* angle separations with snapshots fixed at 100 and the SNR is set to be 0 dB; (b) RMSE *versus* angle separations with snapshots fixed at 200 and the SNR is set to be 0 dB.

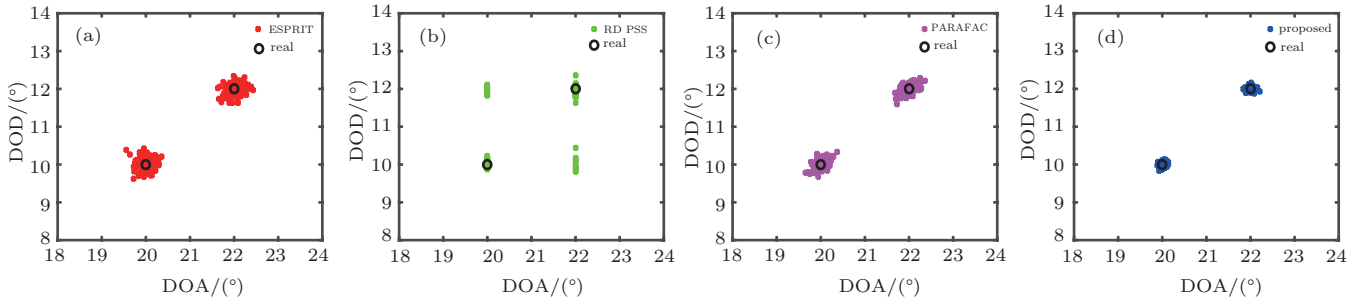


Fig. 8. Scatter comparison of different methods for two closely sources imping from $(\theta_1, \phi_1) = (10°, 20°)$ and $(\theta_2, \phi_2) = (12°, 22°)$ with snapshots = 100 and SNR = 0 dB. (a) Scatter plot of the ESPRIT method, (b) scatter plot of the RD PSS method, (c) scatter plot of the PARAFAC method, and (d) scatter plot of the proposed method.

6. Conclusion

In this paper, an efficient tensor-based estimator has been proposed to deal with the angle parameter estimation of noncircular source in bistatic coprime MIMO radar. In the proposed method, two extended three-order tensor models are constructed by using the noncircular property of the output data. Due to the utilization of the multidimensional structure, the estimated signal subspace matrix exhibits better accuracy by suppressing the effect of the noise. Thereafter, the estimated ambiguous DODs and DOAs can be deterimined via rotational invariance criterion and the angle parameters are automatically paired without extra pairing process. Moreover, the ambiguous angle parameters can be eliminated with the aid of coprime property. And, the closed-form expression of the deterministic CRB for noncircular sources in bistatic coprime MIMO radar is also derived to measure the parameter estimation performance. Theoretical analyses and numerical simulations are carried out to demonstrate that the proposed tensor-based noncircular signal model exhibits excellent estimation performance for coprime MIMO radar compared with other state-of-art methods. In the near future, we will focus on the flexible sparse array design to further improve the angular parameter estimation performance for bistatic MIMO radar system.

References

[1] Wang X P, Wang L Y, Li X M and Bi G A 2017 *Signal Process.* **135** 147

[2] Wang X P, Wan L T, Huang M X, Shen C and Zhang K 2019 *IEEE J. Sel. Topics Signal Process.* **13** 1001

[3] Xie Q P, Pan X Y, Huang M, Chen J Y and Xiao S P 2019 *IEEE Access* **7** 107805

[4] Huang C, Zhang D J, Zhang D L and Teng T T 2014 *Acta Phys. Sin.* **63** 188401 (in Chinese)

[5] Wen F Q, Zhang G and Ben D 2015 *Chin. Phys. B* **24** 110201

[6] Wang T, Zhao Y J, Lai T and Wang J T 2017 *Acta Phys. Sin.* **66** 048401 (in Chinese)

[7] Haimovich M A, Blum R S and Cimini L J 2007 *IEEE Signal Process. Mag.* **25** 116

[8] Li J and Stoica P 2007 *IEEE Signal Process. Mag.* **5** 106

[9] Yan H D, Li J and Liao G S 2008 *EURASIP J. Adv. Signal Process.* **1** 1

[10] Zhang X F, Xu L Y, Xu L and Xu D Z 2010 *IEEE Commun. Lett.* **14** 1161

[11] Bencheikh M L, Wang Y D and He H Y 2010 *Signal Process.* **9** 2723

[12] C D F, Chen B X and Qin G D 2008 *Electron. Lett.* **44** 770

[13] Chen J L, G H and Song W M 2008 *Electron. Lett.* **44** 1422

[14] Wen F Q, Xiong X D, Su J and Zhang Z J 2017 *Signal Process.* **134** 261

[15] Xu B Q and Zhao Y B 2019 *Signal Process.* **157** 88

[16] Li L, Younan N H and Shi X F 2019 *Sensors* **9** 1

[17] Chen J L, Zhou Q G, Li J Q and Zhu Y P 2019 *IET Radar Sonar Navigat.* **13** 1180

[18] Gu Y H, Wang X P, Wan L T, Huang M X, Shen C, Zhang K and Yang Y Q 2019 *IEEE Access* **7** 47972

[19] Yang M L, Sun L, Yuan X and Chen B X 2018 *IEEE Signal Process. Lett.* **25** 40

[20] Qin S, Zhang Y M and Amin M G 2017 *Digit. Signal Process.* **61** 26

[21] Shi J P, Hu G P, Zhang X F and Xiao Y 2018 *Int. J. Electron. Commun.* **94** 339

[22] Zheng G M and Tang J 2016 *Int. J. Electron.* **105** 885

[23] Pal P and Vaidyanathan P P 2010 *IEEE Trans. Signal Process.* **58** 4167

[24] Vaidyanathan P P and Pal P 2011 *IEEE Trans. Signal Process.* **59** 573

[25] Liu C L and Vaidyanathan P P 2016 *IEEE Trans. Signal Process.* **64** 3997

[26] Zhou C W, Shi Z G, Gu Y J and Shen X M 2013 *Proc. IEEE Int. Conf. Wireless Commun. Signal Process.* Hangzhou, October 1

[27] Sun F G, Lan P and Gao B 2015 *Electron. Lett.* **51** 2053

[28] Zhang D, Zhang Y S, Zheng G M, Feng C Q and Tang J 2017 *Electron. Lett.* **53** 1277

[29] Qu Q H, Sun F G, Lan P, Ding G R and Zhang X F 2016 *IEEE Sensors J.* **16** 5660

[30] Zheng W, Zhang X F and Shi Z 2017 *IET Radar Sonar Navigat.* **11** 1581

[31] Zhang X F, Zheng W, Chen W Y and Shi Z 2018 *Multidim Syst Sign Process.* **30** 1

[32] Cai J J, Liu W, Zong R and Wu B 2018 *Signal Process.* **145** 59

[33] Lathauwer L D, Moor B D and Vandewalle J 2000 *SIAM J. Matrix Anal. Appl.* **21** 1253

[34] Kolda T G and Bader B W 2009 *SIAM Rev.* **51** 455

[35] Stoica P and Nehorai A 1989 *IEEE Trans. Acoust. Speech Signal Process.* **37** 720